LETTERS

Blocking VEGFR-3 suppresses angiogenic sprouting and vascular network formation

Tuomas Tammela[1], Georgia Zarkada[1], Elisabet Wallgard[2]*, Aino Murtomäki[1]*, Steven Suchting[3], Maria Wirzenius[1], Marika Waltari[1], Mats Hellström[2], Tibor Schomber[4], Reetta Peltonen[5], Catarina Freitas[3], Antonio Duarte[6], Helena Isoniemi[5], Pirjo Laakkonen[1], Gerhard Christofori[4], Seppo Ylä-Herttuala[7], Masabumi Shibuya[8], Bronislaw Pytowski[9], Anne Eichmann[3], Christer Betsholtz[2] & Kari Alitalo[1]

Angiogenesis, the growth of new blood vessels from pre-existing vasculature, is a key process in several pathological conditions, including tumour growth and age-related macular degeneration[1]. Vascular endothelial growth factors (VEGFs) stimulate angiogenesis and lymphangiogenesis by activating VEGF receptor (VEGFR) tyrosine kinases in endothelial cells[2]. VEGFR-3 (also known as FLT-4) is present in all endothelia during development, and in the adult it becomes restricted to the lymphatic endothelium[3]. However, VEGFR-3 is upregulated in the microvasculature of tumours and wounds[4,5]. Here we demonstrate that VEGFR-3 is highly expressed in angiogenic sprouts, and genetic targeting of VEGFR-3 or blocking of VEGFR-3 signalling with monoclonal antibodies results in decreased sprouting, vascular density, vessel branching and endothelial cell proliferation in mouse angiogenesis models. Stimulation of VEGFR-3 augmented VEGF-induced angiogenesis and sustained angiogenesis even in the presence of VEGFR-2 (also known as KDR or FLK-1) inhibitors, whereas antibodies against VEGFR-3 and VEGFR-2 in combination resulted in additive inhibition of angiogenesis and tumour growth. Furthermore, genetic or pharmacological disruption of the Notch signalling pathway led to widespread endothelial VEGFR-3 expression and excessive sprouting, which was inhibited by blocking VEGFR-3 signals. Our results implicate VEGFR-3 as a regulator of vascular network formation. Targeting VEGFR-3 may provide additional efficacy for anti-angiogenic therapies, especially towards vessels that are resistant to VEGF or VEGFR-2 inhibitors.

During late embryogenesis and in the adult, blood vessels form primarily by angiogenesis—that is, sprouting from pre-existing vessels. VEGF potently promotes angiogenesis and is indispensable for vascular development[6,7], whereas VEGFR-2 tyrosine kinase is the primary receptor transmitting VEGF signals in endothelial cells[8,9]. Angiogenic sprouting involves specification of subpopulations of endothelial cells into tip cells that respond to VEGF guidance cues and into stalk cells that follow the tip cells and proliferate to form the vascular network[10]. Recent evidence indicates that VEGF induces the Notch ligand Delta-like 4 (DLL4) in the tip cells, which leads to suppression of excess sprouts in adjacent endothelial cells[11–17].

VEGFR-3 is activated by VEGF-C and VEGF-D (also known as FIGF), which can also stimulate VEGFR-2 after proteolytic processing (reviewed in ref. 18). Furthermore, VEGF-C has been shown to induce the formation and activation of VEGFR-2–VEGFR-3 heterodimers[19]. *Vegfr3*-gene-targeted mice exhibit marked defects in arterial–venous remodelling of the primary vascular plexus, resulting in lethality by embryonic day (E)10.5 (ref. 20). Correspondingly, knockdown of the *Vegfr3* homologue in zebrafish results in defective segmental artery morphogenesis[21]. We recently observed that blocking antibodies against VEGFR-3 inhibit tumour growth by inhibiting angiogenesis[22]. These results suggested that VEGFR-3 signalling is required for both developmental and tumour angiogenesis, raising the question of how VEGFR-3 regulates this process.

We validated vascular VEGFR-3 expression in tumours by growing syngeneic tumours in *Vegfr3*[+/LacZ] mice, which allows visualization of *Vegfr3*-expressing cells using the β-galactosidase reporter driven by the *Vegfr3* promoter. Blood vessels within the tumour tissue showed *Vegfr3* promoter activity in grafted B16 melanomas (Fig. 1a, arrows) and Lewis lung carcinomas (data not shown), but not in the adjacent peritoneum. We also detected blood vascular VEGFR-3 expression in human colon carcinoma metastases of the liver, in all three human tumour xenografts analysed, and in transgenic Rip1Tag2 mouse insulinomas (Supplementary Fig. 1). Notably, VEGFR-3 immunostaining in the tumours was prominent in endothelial sprouts (Supplementary Fig. 1c–e). Angiogenic vessels positive for VEGFR-3 but negative for the lymphatic vessel marker LYVE-1 were also found in developing ovarian follicles of superovulated mice (Supplementary Fig. 2). These data indicated that VEGFR-3 is expressed specifically in blood vessels undergoing angiogenesis.

Because blood vessels are disorganized in tumour tissues, we studied VEGFR-3 expression in the mouse retina, where new vessels form in an organized and directional manner during the postnatal period by sprouting angiogenesis that proceeds centrifugally from the optic disc[10]. VEGFR-3 was strongly expressed in the angiogenic vessel front during the early postnatal period (days 1–7; Fig. 1b and Supplementary Fig. 3), but not in mature vessels at postnatal day (P)28 (Supplementary Fig. 3b). VEGFR-3 was also weakly expressed in the veins and venules (Fig. 1b, c and Supplementary Fig. 3), reflecting the pattern observed during early vascular development[20]. High-resolution analysis revealed that the β-galactosidase reporter driven by the VEGFR-3 promoter localized to the leading tip cells of endothelial sprouts (Fig. 1c and Supplementary Fig. 3c), whereas immunofluorescence analysis by confocal microscopy demonstrated

that VEGFR-3 is present in the filopodial extensions of the tip cells (Fig. 1d), where previous studies have reported prominent VEGFR-2 expression[10,16]. We detected VEGF-C protein and promoter activity in leukocytes that were positioned in the region of vascular network formation (Supplementary Fig. 4a–e). VEGF-C bound to endothelial cells was detected by immunostaining (Supplementary Fig. 4a, b).

In developing embryos, the most intense VEGFR-3 staining localized to areas of active angiogenesis at E8.5–E9.5 (Fig. 1e, arrowheads). High-resolution analysis by immunofluorescence indicated intense expression in actively sprouting intersomitic vessels, whereas few sprouts and low levels of VEGFR-3 were detected in the adjacent dorsal aorta at E9.25 (Fig. 1f). VEGF-C expression was detected in the endothelium of actively growing intersomitic vessels at E9.0 and E9.5
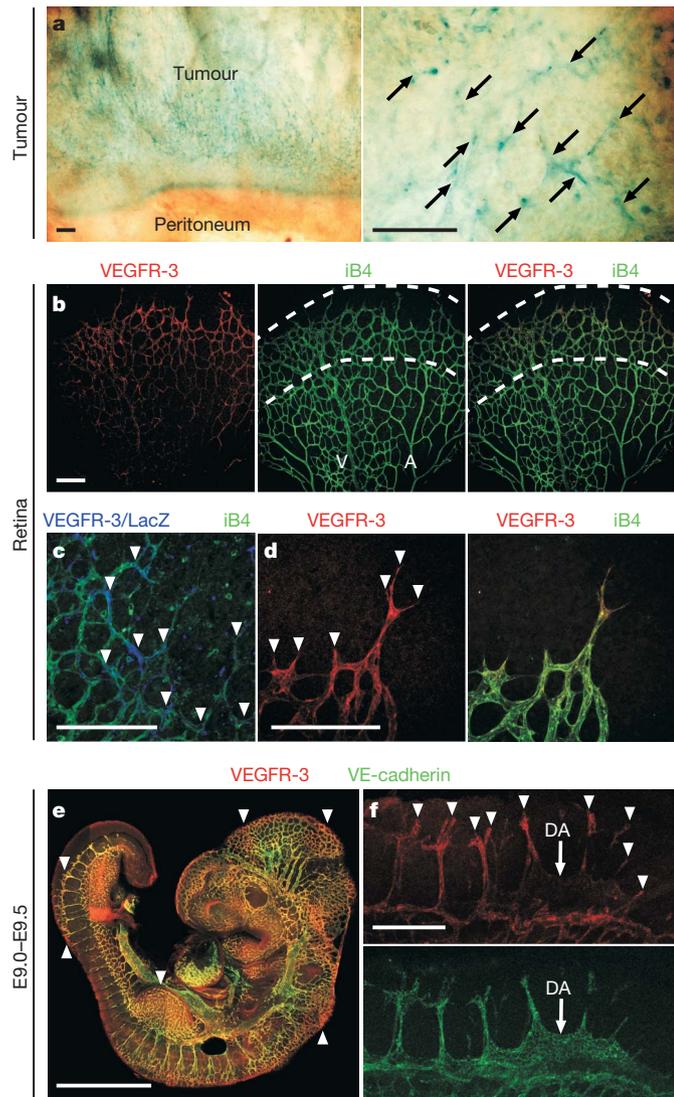

Figure 1 | VEGFR-3 is expressed in the tumour vasculature and localizes to endothelial tip cells. a, VEGFR-3 expression (arrows, blue) detected by X-gal staining in a syngeneic B16 melanoma implanted subcutaneously into a $Vegfr3^{+/LacZ}$ heterozygous mouse. The peritoneal membrane, which contains normal blood vessels, has no staining. **b**, VEGFR-3 staining (red) of a mouse retina at P5. Blood vessels are visualized with isolectin B4 staining (iB4, green). A, artery; V, vein. **c**, A single confocal section showing VEGFR-3 (blue) after X-gal staining, and isolectin B4 (green) in the angiogenic front at P5. **d**, VEGFR-3 (red) in blood vessels (green) at P5 in the angiogenic front. Arrowheads point to regions of most intense VEGFR-3 expression in **c** and **d. e**, VEGFR-3 (red) and VE-cadherin (green) in a mouse embryo at E9.5. **f**, Intersomitic vessels of a mouse embryo at E9.25. VEGFR-3-positive (red) sprouts are indicated with arrowheads. VE-cadherin staining is in green. DA, dorsal aorta in **f**. Scale bars, 100 μm, except in **e** (which is 500 μm).

in $Vegfc^{+/LacZ}$ embryos (Supplementary Fig. 4f–i and data not shown). Interestingly, the vasculature of the head appeared less complex at E8.5 (Supplementary Fig. 5), and intersomitic vessels were smaller and had fewer sprouts at E9.0 in $Vegfr3$-gene-targeted embryos compared to wild-type littermates (Supplementary Fig. 6). VEGFR-2 expression was not affected by loss of $Vegfr3$ (Supplementary Fig. 7), indicating that VEGFR-3 signalling is directly required for vascular development.

To inhibit VEGFR-3 signalling in the postnatal retina, newborn pups were given monoclonal antibodies that specifically block ligand binding to VEGFR-3. Antibodies that block VEGFR-2 were used as a positive control for angiogenesis inhibition, and non-specific rat immunoglobulin G (IgG) as a negative control. The vascular network appeared less dense in retinas of pups that were given anti-VEGFR-3 antibodies, whereas only rudimentary vessels were found in pups injected with anti-VEGFR-2 antibodies (Fig. 2a). Interestingly, when both VEGFR-2 and VEGFR-3 antibodies were administered in combination, a more marked reduction of vascular surface area and endothelial sprouts was obtained (Fig. 2b–e), suggesting that VEGFR-3 signalling in part compensates for lack of VEGFR-2 signalling. Notably, blocking VEGFR-3 appeared to most markedly affect the number of sprouts and branching points (Fig. 2c, d). However, we also detected a decrease in the number of proliferating endothelial cells in mice that received VEGFR-3-blocking antibodies (Fig. 2e), which is in line with findings indicating that VEGFR-3 signals promote the proliferation and survival of endothelial cells in culture[23,24].

VEGFR-3 antibodies or an adenovirally delivered soluble VEGFR-3–Ig fusion protein[25] also markedly reduced the number of VEGFR-3-positive endothelial sprouts in lung carcinoma xenografts (Fig. 2f, g and data not shown), suggesting that VEGFR-3 inhibitors inhibit angiogenesis by suppressing endothelial sprouting. The combination of VEGFR-3 and VEGFR-2 antibodies for 6 days led to a significant decrease in blood vessel density in LNM35 and B16 tumours when compared to administration of either antibody alone (Fig. 2h and not shown). Importantly, the combination of VEGFR-3 and VEGFR-2 antibodies reduced vascular surface area 45%, viable tumour area 32% and tumour growth 41% more effectively than blockade of VEGFR-2 alone (Fig. 2j–l).

To elucidate how VEGFR-3 expression is induced during angiogenesis, we used a model with less confounding factors than in tumours. Expression of human VEGF or VEGF-E—a VEGFR-2-specific ligand—in the skin under the control of the keratin 14 promoter ($K14$-VEGF or $K14$-VEGF-E, respectively, induced marked blood vessel hyperplasia and upregulation of VEGFR-3 in cutaneous blood vessels, whereas the vessels were VEGFR-3-negative in wild-type littermates (Fig. 3a and Supplementary Fig. 8a). Surprisingly, both vascular phenotypes were greatly attenuated in $K14$-VEGF;$K14$-VEGFR-3–Ig and $K14$-VEGF-E;$K14$-VEGFR-3–Ig compound transgenic mice (Fig. 3a, b and Supplementary Fig. 8b, c), indicating that VEGFR-3 signals contributed to the excess angiogenesis. In contrast, the blood vessels of $K14$-VEGFR-3–Ig single-transgenic mice appeared normal, as previously published (Fig. 3a, b)[25]. These results suggest that the angiogenic VEGFR-3 signal is active predominantly during settings of angiogenic invasion of tissues, such as during early embryonic development, in the postnatal retina, and in tumours.

To dissect the VEGFR-2 and VEGFR-3 pathways *in vivo*, we used adenoviral gene transfer vectors in the mouse ear skin for overexpression of VEGFs. When VEGF or VEGF-E was expressed together with mouse VEGF-D—a VEGFR-3-specific ligand[26]—we observed a significant increase in angiogenesis when compared to expression of these factors alone (Fig. 3c, Supplementary Fig. 9). However, mouse VEGF-D was not able to induce angiogenesis on its own, suggesting that blood vessels need to be primed by VEGFR-2 signals to become responsive to VEGFR-3 ligands (Fig. 3c and Supplementary Fig. 9). In a reversed experiment, we overexpressed both VEGF and VEGF-C, which are both commonly expressed in tumours, in the ear skin.

2

Blocking both VEGFR-3 and VEGFR-2 with monoclonal antibodies normalized the vasculature, whereas excess vessels were observed in ears treated with either antibody alone (Fig. 3d, e), indicating that VEGFR-3 signals can sustain a low degree of angiogenesis even in the presence of VEGFR-2 blockers.

Endothelial Notch activation by DLL4 has recently been shown to suppress excess sprouts in angiogenic vessels[13–16]. Conversely, disruption of a downstream Notch signalling component in zebrafish

Figure 2 | VEGFR-3-function-blocking antibodies inhibit angiogenic sprouting. a–e, Analysis of changes in retinal microvasculature after administration of monoclonal antibodies. Isolectin B4 staining of retinal vessels of pups injected once daily with anti-VEGFR-3 antibodies (R3, $n = 22$), anti-VEGFR-2 antibodies (R2, $n = 18$), VEGFR-3 and VEGFR-2 antibodies in combination (R3 + 2, $n = 12$) or control rat IgG ($n = 24$) during P0–P5. Isolectin B4-positive surface area density (**b**), number of vessel branch points (**c**), number of sprouts (**d**), and number of BrdU-positive endothelial cells (**e**) per mm^2. **f**, NCI-H460-LNM35 tumour xenografts after treatment with the VEGFR-3-blocking antibody (R3) or control IgG. VEGFR-3-positive endothelial sprouts (arrowheads, red) and PECAM-1 staining (green) are shown. **g**, Quantitative analysis of VEGFR-3-positive endothelial sprouts in the microvasculature of the tumours after administration of anti-VEGFR-3 antibodies (R3–Ab, $n = 5$), adenoviral VEGFR-3–Ig (R3–Ig, $n = 4$) or rat IgG ($n = 8$). **h**, Quantification of PECAM-1-positive blood vessel surface area in B16 and LNM35 tumours 6 days after treatment ($n \geq 4$ tumours per group). **i–l**, Immunostaining of PECAM-1 (green; **i**), quantification of PECAM-1 positive surface area (**j**) and viable tumour area (**k**) in LNM35 tumour xenografts treated for 18 days with monoclonal antibodies ($n = 6$–8 per group). **o**, Growth of LNM35 tumour xenografts treated with the indicated monoclonal antibodies ($n = 8$ per group). Asterisk, $P < 0.05$. Scale bars, 100 μm. All error bars indicate + s.e.m.

resulted in increased sprouting and induced *Vegfr3* (*Flt4*) expression[15]. To study whether Notch regulates VEGFR-3 expression, we treated newborn pups with DAPT, a γ-secretase inhibitor that blocks the Notch signalling pathway. Conversely, we activated the Notch pathway with a small peptide mimetic of the Notch ligand jagged 1 (JAG1; ref. 13). VEGFR-3 expression was not restricted to the angiogenic front in retinas of mice treated with DAPT for 12–48 h (Fig. 4a, b and Supplementary Fig. 10a–c), whereas mice that received JAG1 displayed diminished vascular VEGFR-3 expression (Fig. 4a, b and Supplementary Fig. 10c–e). Furthermore, DAPT induced and JAG1 suppressed *Vegfr3* transcription in the retinas (Fig. 4c), suggesting that the Notch pathway downregulates VEGFR-3 expression *in vivo*, although *VEGFR3* may initially be induced by Notch activation at least in cultured cells[27]. In our experiments, *Vegfr3* mRNA levels did not change until the 12 h time point, whereas *Pdgfb* and *Nrarp*, used as controls for Notch activity, already responded at 6 h (Fig. 4c). This suggests that Notch downregulates *Vegfr3* by means of intermediate effectors such as the transcriptional repressors HEY1, HEY2 or HES1 (ref. 17), which were downregulated at 12 h, when *Vegfr3* upregulation in response to DAPT was first observed (Supplementary Fig. 10f). DAPT also induced VEGFR-3 in tumour blood vessels (Supplementary Fig. 10g), and administration of either VEGFR-3- or VEGFR-2-blocking antibodies suppressed vascular hyperplasia in tumours during DAPT treatment. Additive inhibition of angiogenesis was not seen when combining either receptor-blocking antibody and DAPT (Fig. 4d and data not shown).

Our data indicate that VEGFR-2 activation induces VEGFR-3 (Fig. 3), whereas previous reports have demonstrated that VEGF induces DLL4 in tip cells by means of VEGFR-2 (refs 13, 14 and 16). We found increased VEGFR-3 protein and mRNA levels in the retinas of DLL4 heterozygous pups that survive but exhibit decreased Notch signalling in endothelial cells (Fig. 4e–g), indicating that DLL4 downregulates VEGFR-3 by means of Notch. Intraocularly injected VEGFR-3 antibodies partially rescued the hyperactive sprouting
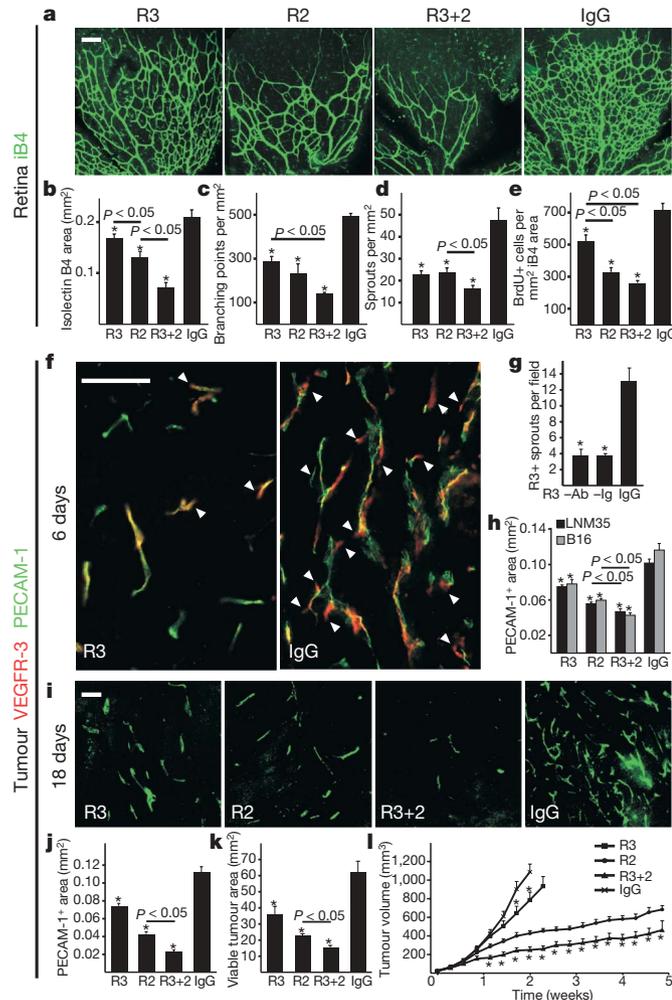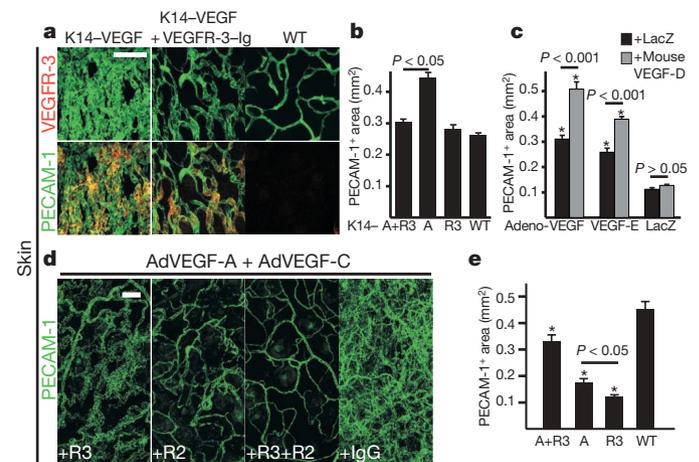

Figure 3 | Regulation and activation of VEGFR-3 by VEGF family ligands. a, b, VEGFR-3 (red) and PECAM-1 (green) in the skin of transgenic K14–VEGF;K14–VEGFR-3–Ig (A + R3, $n = 5$), K14–VEGF (A, $n = 6$), K14–VEGFR-3–Ig (R3, $n = 3$) mice, or in wild-type littermate mice (WT, $n = 4$) at P2. Epigastric skin in the ventral midline lacking lymphatic vessels is shown in **a**. The top row shows PECAM-1 staining, and the bottom row shows PECAM-1 and VEGFR-3 double staining. Quantification of the PECAM-1-positive vessel area in transgenic versus wild-type mice (**b**). **c**, Quantification of the PECAM-1-positive vessel area in ears transduced with the indicated adenoviral vectors. Representative images of the samples are shown in Supplementary Fig. 8. **d, e**, Analysis of blood vessels (PECAM-1, green) in ears transduced with adenoviral (Ad) vectors encoding VEGF and VEGF-C, followed by treatment with the indicated monoclonal antibodies (**d**). Quantification of the PECAM-1-positive vessel surface area in the ears (**e**). Asterisk, $P < 0.05$. Scale bars, 100 μm (**a, d**); 10 μm (**f**). All error bars indicate + s.e.m.

phenotype seen in DLL4 heterozygotes, as seen by reduced numbers of filopodia and decreased filopodal length (Supplementary Fig. 11a–c). VEGFR-3 antibodies administered during treatment with DAPT also partially inhibited the hyperactive sprouting/branching phenotype induced by Notch inhibition in the retina (Supplementary Fig. 11d, e). These results suggest that upregulation and activation of VEGFR-3 has a functional role in sprouting angiogenesis, and that VEGFR-3 is an important effector of the vascular phenotype resulting from Notch inhibition.

In recent years, the development of angiogenesis inhibitors has focused on the VEGF/VEGFR-2 system. These inhibitors have shown promising efficacy in the clinic in the treatment of tumours and ocular disease, but tumours in particular may eventually become resistant to VEGF/VEGFR-2 inhibitors[28]. Our results indicate that angiogenic sprouting is impaired without VEGFR-3 signals, and suggest that VEGFR-3 may drive angiogenesis even in conditions of therapeutic targeting of VEGFR-2 (Supplementary Fig. 12). VEGF-C is produced by leukocytes, such as macrophages[29], whereas robust VEGF-C production has been detected in a variety of tumour cell lines and in human tumours, which correlates with increased propensity for lymphatic metastasis in some human tumours[4,22,30]. In light of our results, a significant biological role for VEGF-C in the tumour setting may be to augment angiogenesis and sustain tumour growth in addition to actively promoting lymphatic metastasis. Thus, our findings elucidate a previously unknown and important regulatory system for angiogenesis, and suggest a new target for anti-angiogenic therapies.

METHODS SUMMARY

Animal procedures. All animal experiments were approved by the Committee for Animal Experiments in the District of Southern Finland. *Vegfr3*-gene-targeted or wild-type E8.5–E11.5 mouse embryos, *Vegfr3*$^{+/LacZ}$, *Vegfc*$^{+/LacZ}$, *Dll4*$^{+/LacZ}$ or wild-type neonatal pups, or adult K14-transgenic or wild-type mice were used for the experiments. Tumour-bearing adult mice or neonatal pups were intraperitoneally or subcutaneously administered VEGFR-3, VEGFR-2, VEGFR-3 + VEGFR-2, or control monoclonal antibodies, and/or DAPT, JAG1, scrambled control peptide (SC-JAG1) or vehicle. Alternatively, tumour-bearing mice were injected intravenously with adenoviruses encoding VEGFR-3–Ig or β-galactosidase as a control. Ears of adult immunodeficient nu/nu mice were injected with adenoviral vectors encoding VEGF family growth factors or control.

Tissue imaging. Embryos, postnatal retinas or skin were processed for whole-mount staining, whereas tumours were cut into 50-μm sections for immunostaining. Proliferating or hypoxic cells were identified by injection of bromodeoxyuridine or pimonidazole, respectively, 1–2 h before euthanasia. Commercially available or previously published antibodies were used for immunostaining according to standard protocols. Samples were imaged using a Zeiss Axiovert epifluorescence or a Zeiss LSM 510 Meta/LIVE5 confocal laser-scanning microscope.

Molecular analyses. Gene expression levels were analysed from RNA extracted from postnatal retinas at P5 by quantitative real-time PCR, as described previously[13].

Quantitative analysis. At least three animals were analysed in each time point and treatment. Statistical analysis was carried out using the unpaired Student's *t*-test or one-way analysis of variance (ANOVA).

Full Methods and any associated references are available in the online version of the paper at www.nature.com/nature.
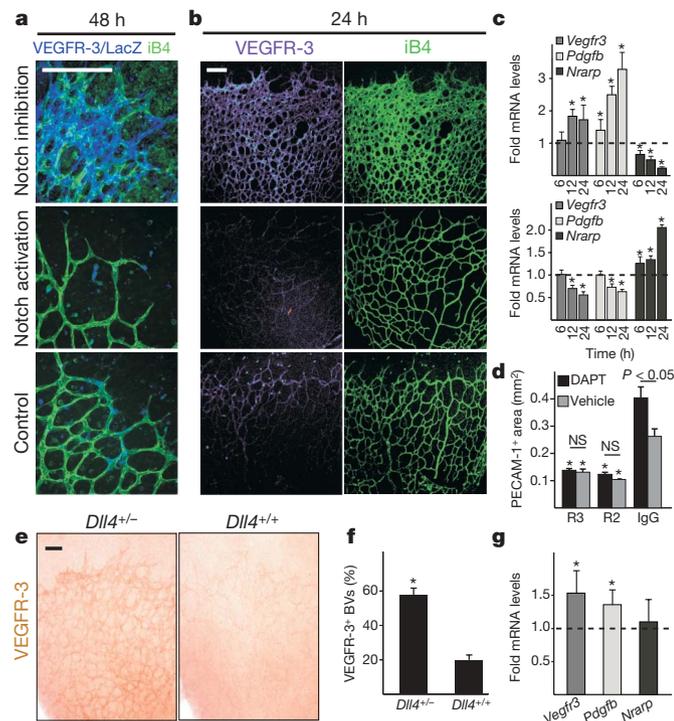
1. Carmeliet, P. Angiogenesis in life, disease and medicine. *Nature* **438**, 932–936 (2005).
2. Ferrara, N., Gerber, H. P. & LeCouter, J. The biology of VEGF and its receptors. *Nature Med.* **9**, 669–676 (2003).
3. Kaipainen, A. *et al.* Expression of the fms-like tyrosine kinase 4 gene becomes restricted to lymphatic endothelium during development. *Proc. Natl Acad. Sci. USA* **92**, 3566–3570 (1995).
4. Valtola, R. *et al.* VEGFR-3 and its ligand VEGF-C are associated with angiogenesis in breast cancer. *Am. J. Pathol.* **154**, 1381–1390 (1999).
5. Paavonen, K., Puolakkainen, P., Jussila, L., Jahkola, T. & Alitalo, K. Vascular endothelial growth factor receptor-3 in lymphangiogenesis in wound healing. *Am. J. Pathol.* **156**, 1499–1504 (2000).
6. Ferrara, N. *et al.* Heterozygous embryonic lethality induced by targeted inactivation of the VEGF gene. *Nature* **380**, 439–442 (1996).
7. Carmeliet, P. *et al.* Abnormal blood vessel development and lethality in embryos lacking a single VEGF allele. *Nature* **380**, 435–439 (1996).
8. Shalaby, F. *et al.* Failure of blood island formation and vasculogenesis in Flk-1-deficient mice. *Nature* **376**, 62–66 (1995).
9. Gille, H. *et al.* Analysis of biological effects and signaling properties of Flt-1 (VEGFR-1) and KDR (VEGFR-2). A reassessment using novel receptor-specific vascular endothelial growth factor mutants. *J. Biol. Chem.* **276**, 3222–3230 (2001).
10. Gerhardt, H. *et al.* VEGF guides angiogenic sprouting utilizing endothelial tip cell filopodia. *J. Cell Biol.* **161**, 1163–1177 (2003).
11. Noguera-Troise, I. *et al.* Blockade of Dll4 inhibits tumour growth by promoting non-productive angiogenesis. *Nature* **444**, 1032–1037 (2006).
12. Ridgway, J. *et al.* Inhibition of Dll4 signalling inhibits tumour growth by deregulating angiogenesis. *Nature* **444**, 1083–1087 (2006).
13. Hellstrom, M. *et al.* Dll4 signalling through Notch1 regulates formation of tip cells during angiogenesis. *Nature* **445**, 776–780 (2007).
14. Lobov, I. B. *et al.* Delta-like ligand 4 (Dll4) is induced by VEGF as a negative regulator of angiogenic sprouting. *Proc. Natl Acad. Sci. USA* **104**, 3219–3224 (2007).
15. Siekmann, A. F. & Lawson, N. D. Notch signalling limits angiogenic cell behaviour in developing zebrafish arteries. *Nature* **445**, 781–784 (2007).
16. Suchting, S. *et al.* The Notch ligand Delta-like 4 negatively regulates endothelial tip cell formation and vessel branching. *Proc. Natl Acad. Sci. USA* **104**, 3225–3230 (2007).
17. Roca, C. & Adams, R. H. Regulation of vascular morphogenesis by Notch signaling. *Genes Dev.* **21**, 2511–2524 (2007).

Figure 4 | Notch signalling downregulates VEGFR-3 in endothelial cells.
a–c, Analysis of the effects of the γ-secretase inhibitor DAPT (Notch inhibition) or the JAG1 peptide (Notch activation) on VEGFR-3 expression in the postnatal mouse retina. VEGFR-3 (blue pseudocolour) in the retinas of *Vegfr3*$^{+/LacZ}$ heterozygous mice (**a**), and VEGFR-3 (purple rainbow colour) and isolectin B4 (green) staining (**b**), in wild type retinas at P5 are shown. Quantification of changes in *Vegfr3*, *Pdgfb* and *Nrarp* mRNA levels after DAPT (upper graph) or JAG1 (lower graph) administration is shown in **c**. The dashed line indicates the relative mRNA levels in vehicle- or SC-JAG1-treated controls ($n \geq 3$ mice per group, error bars indicate $\pm$ s.d.).
d, Quantification of the PECAM-1-positive surface area in tumours treated with DAPT or vehicle and the indicated monoclonal antibodies ($n \geq 4$ tumours per group; error bars indicate + s.e.m.). **e,** Simultaneous VEGFR-3 immunostaining of *Dll4*$^{+/-}$ and wild-type littermate retinas.
f–g, Quantification of the VEGFR-3-positive surface area (**f**) and changes in *Vegfr3*, *Pdgfb* and *Nrarp* mRNA levels (**g**) in *Dll4*$^{+/-}$ and *Dll4*$^{+/+}$ pups ($n \geq 3$ mice per group). Error bars indicate $\pm$ s.e.m. in **f** and $\pm$ s.d. in **g**. NS, not statistically significant; asterisk, $P < 0.05$; scale bars, 100 μm.

18. Alitalo, K., Tammela, T. & Petrova, T. V. Lymphangiogenesis in development and human disease. *Nature* **438**, 946–953 (2005).

19. Dixelius, J. *et al.* Ligand-induced vascular endothelial growth factor receptor-3 (VEGFR-3) heterodimerization with VEGFR-2 in primary lymphatic endothelial cells regulates tyrosine phosphorylation sites. *J. Biol. Chem.* **278**, 40973–40979 (2003).

20. Dumont, D. J. *et al.* Cardiovascular failure in mouse embryos deficient in VEGF receptor-3. *Science* **282**, 946–949 (1998).

21. Covassin, L. D., Villefranc, J. A., Kacergis, M. C., Weinstein, B. M. & Lawson, N. D. Distinct genetic interactions between multiple Vegf receptors are required for development of different blood vessel types in zebrafish. *Proc. Natl Acad. Sci. USA* **103**, 6554–6559 (2006).

22. Laakkonen, P. *et al.* Vascular endothelial growth factor receptor 3 is involved in tumor angiogenesis and growth. *Cancer Res.* **67**, 593–599 (2007).

23. Veikkola, T. *et al.* Intrinsic versus microenvironmental regulation of lymphatic endothelial cell phenotype and function. *FASEB J.* **17**, 2006–2013 (2003).

24. Goldman, J. *et al.* Cooperative and redundant roles of VEGFR-2 and VEGFR-3 signaling in adult lymphangiogenesis. *FASEB J.* **21**, 1003–1012 (2007).

25. Makinen, T. *et al.* Inhibition of lymphangiogenesis with resulting lymphedema in transgenic mice expressing soluble VEGF receptor-3. *Nature Med.* **7**, 199–205 (2001).

26. Baldwin, M. E. *et al.* The specificity of receptor binding by vascular endothelial growth factor-D is different in mouse and man. *J. Biol. Chem.* **276**, 19166–19171 (2001).

27. Shawber, C. J. *et al.* Notch alters VEGF responsiveness in human and murine endothelial cells by direct regulation of VEGFR-3 expression. *J. Clin. Invest.* **117**, 3369–3382 (2007).

28. Ferrara, N. & Kerbel, R. S. Angiogenesis as a therapeutic target. *Nature* **438**, 967–974 (2005).

29. Baluk, P. *et al.* Pathogenesis of persistent lymphatic vessel hyperplasia in chronic airway inflammation. *J. Clin. Invest.* **115**, 247–257 (2005).

30. Stacker, S. A., Achen, M. G., Jussila, L., Baldwin, M. E. & Alitalo, K. Lymphangiogenesis and cancer metastasis. *Nature Rev. Cancer* **2**, 573–583 (2002).

Supplementary Information is linked to the online version of the paper at www.nature.com/nature.

Author Contributions T.T. designed, directed and performed embryo, retina, mouse ear and xenograft experiments, immunohistochemistry and data analysis, interpreted results and wrote the paper; G.Z. performed xenograft experiments, immunohistochemistry, electron microscopy and ELISA, analysed data and interpreted results; E.W. designed and performed qRT–PCR and data analysis, and interpreted results; A.M. performed embryo and retina experiments, immunohistochemistry, and data analysis; S.S. performed intraocular injections and immunohistochemistry, analysed data and interpreted results; M. Wirzenius designed and performed mouse ear experiments and immunohistochemistry, analysed data and interpreted results; M. Waltari performed xenograft experiments, immunohistochemistry and data analysis; M. H. directed experiments and interpreted results; T.S. performed Rip1Tag2 tumour experiments, analysed data and interpreted results; R.P. performed immunohistochemistry and analysed data; C.F. performed intraocular injections; A.D. provided the *Dll4*$^{+/-}$ mice; H.I. performed surgery and provided clinical tumour samples; P.L. directed experiments and interpreted results; G.C. directed experiments and interpreted results; S.Y.-H. developed and provided adenovirus vectors; M.S. generated and provided K14–VEGF and K14–VEGF-E transgenic mice; B.P. generated and provided monoclonal VEGFR function-blocking antibodies; A.E. directed experiments and interpreted results; C.B. designed experiments, interpreted results and helped write the paper; K.A. designed experiments, interpreted results and wrote the paper.

METHODS

Mice and tissues. The study was approved by the Committee for Animal Experiments of the District of Southern Finland. For tumour injections and before they were killed, the mice were anesthetized with intraperitoneal injections of xylazine ($10 \, mg \, kg^{-1}$) and ketamine ($50 \, mg \, kg^{-1}$). The $Vegfr3^{+/LacZ}$ (ref. 20), $Vegfc^{+/LacZ}$ (ref. 31) and $Dll4^{+/LacZ}$ (ref. 32) knock-in mice, as well as the K14–VEGF-E (ref. 33), K14–VEGF$_{165}$ (ref. 34), K14–VEGFR-3–Ig (ref. 25) and Rip1Tag2 (refs 35 and 36) transgenic mouse lines, were as published previously. T-cell-deficient Balb/c nu/nu or NMRI nu/nu mice (Taconic) were used for the tumour xenografting experiments. Neonatal wild-type mice in the NMRI, CD1 or C57black background, $Vegfc^{+/LacZ}$ mice in the NMRI background, $Vegfr3^{+/LacZ}$ and $Vegfr3^{LacZ/LacZ}$ mice in the ICR background, or $Dll4^{+/LacZ}$ mice in the CD1 background were used for the experiments. Twenty-four-day-old wild-type female FVB/n mice were used for superovulation experiments. After killing the mice, tissues were immersed in 4% paraformaldehyde, washed in phosphate buffered saline (PBS) and then processed for whole-mount staining, immersed in OCT medium (Tissue Tek) or embedded in paraffin.

Analysis of postnatal angiogenesis in the mouse retina. Neonatal wild-type mice in the NMRI background were intraperitoneally or subcutaneously injected with $50 \, mg \, kg^{-1} \, d^{-1}$ of anti-VEGFR-3 (mF4-31C1, ref. 37) or anti-VEGFR-2 (DC101, ref. 38) monoclonal antibodies, which inhibit ligand binding to mouse VEGFR-3 or VEGFR-2, respectively. Non-specific rat IgG (Dako) was used as a control. Alternatively, $50 \, mg \, kg^{-1} \, d^{-1}$ anti-VEGFR-3 plus $50 \, mg \, kg^{-1} \, d^{-1}$ anti-VEGFR-2 were given in combination. Treatment with the antibodies was continued from P0 until P5, when the mice were killed and their eyes collected for analysis. Intraocular injections were carried out as described previously[16], and the pups were killed 5 h after injection. The γ-secretase inhibitor DAPT (N-[N-(3,5-difluorophenacetyl-L-alanyl)]-S-phenylglycine t-bytyl ester, Sigma)[39] was dissolved in 10% ethanol and 90% sunflower oil (Sigma), and injected subcutaneously at $100 \, mg \, kg^{-1}$ in a volume of $10 \, \mu l \, g^{-1}$ into P2 pups twice daily. The vehicle was used as a negative control. The small peptide mimetic of the Notch ligand JAG1 or SC-JAG1 (Thermo Scientific) was dissolved in 50% dimethyl-sulphoxide (DMSO) and 50% sterile water, and was administered subcutaneously at $10 \, mg \, kg^{-1}$ (refs 13, 40). Pups were killed on P5, 6 h, 12 h, 24 h or 48 h after administration of DAPT, JAG1, SC-JAG1 or vehicle at 12-h intervals. Alternatively, the mice were given DAPT four times and the monoclonal antibodies twice over a period of 48 h. For labelling of proliferating cells, the mice were given an intraperitoneal injection of bromodeoxyuridine ($1 \, mg \, kg^{-1}$, Sigma) 2 h before they were killed.

Transduction of the mouse ear skin with adenoviral gene transfer vectors. Adenoviruses encoding human VEGF$_{165}$ (ref. 41), human full-length VEGF-C (ref. 41), mouse VEGF-D or the Orf(NZ7) virus-encoded VEGF-E (ref. 42) were injected intradermally into the ears of immunodeficient nu/nu mice in the following combinations: VEGF + LacZ, VEGF + mVEGF-D, VEGF-E + LacZ, VEGF-E + mVEGF-D or mVEGF-D + LacZ, or LacZ alone. AdLacZ (ref. 41) was used as a negative control. 10^8 plaque-forming units (p.f.u.) of each virus (altogether 2×10^8 p.f.u.) were injected in a volume of $50 \, \mu l$. The ears were harvested 6 days after injection and processed for whole-mount analysis, as described previously[43]. Alternatively, 10^8 p.f.u. of both AdVEGF and AdVEGF-C were injected on day 0. The mice were given anti-VEGFR-3 ($40 \, mg \, kg^{-1}$), anti-VEGFR-2 ($40 \, mg \, kg^{-1}$), anti-VEGFR-3 and anti-VEGFR-2 ($40 + 40 \, mg \, kg^{-1}$) in combination, or IgG ($40 \, mg \, kg^{-1}$) on days 4 and 6. The mice were killed on day 8 and ears were collected for analysis.

Human samples. Patients diagnosed with disseminated adenocarcinoma of the colon underwent a standard chemotherapy regimen, followed by partial resection of the liver to eradicate metastases. Samples from the interface between normal and tumour tissue were immediately immersed in 4% paraformaldehyde overnight (12–16 h) at $+4 \, °C$, washed in PBS, incubated in 25% sucrose overnight at $+4 \, °C$, embedded in optimal cutting temperature (OCT) medium and frozen. $50 \, \mu m$ sections were used for staining. The study was approved by the Ethical Committee of The Hospital District of Helsinki and Uusimaa according to the guidelines of the Helsinki declaration. Informed consent was obtained from the patients.

Tumour cell lines, xenografts and treatments. NCI-H460-LNM35 cells (LNM35), a sub-line of NCI-H460-N15, a human large-cell carcinoma of the lung[44] (a gift from T. Takahashi), MKN45 human gastric carcinoma cells[45] (a gift from A. Ristimäki), B16 mouse melanoma or Lewis mouse lung carcinoma cells were maintained in RPMI-1640 medium, whereas the G401 kidney cancer cells (ATCC CRL-1441) were grown in DMEM. Both media were supplemented with $2 \, mM$ L-glutamine, penicillin ($100 \, U \, ml^{-1}$), streptomycin ($100 \, \mu g \, ml^{-1}$) and 10% fetal bovine serum (Autogen Bioclear).

The LNM35, MKN45 and G401 xenografts, as well as the B16 and LLC syngeneic grafts, were made by injecting $0.5–5 \times 10^6$ cells into the subcutaneous space in the abdominal flank of immunodeficient mice. For experiments involving antibody treatment, 10^6 LNM35 cells or 5×10^5 B16 cells were injected into the subcutaneous space above the abdomen of each mouse. Tumours were allowed to reach a volume of approximately $50 \, mm^3$ and then the mice were randomized by tumour volume into treatment groups. The tumour-bearing mice were treated with anti-VEGFR-3, anti-VEGFR-2 or non-specific rat IgG (Dako) every other day by intraperitoneal injection ($40 \, mg \, kg^{-1}$). Mice that received anti-VEGFR-3 and anti-VEGFR-2 in combination were given $40 \, mg \, kg^{-1}$ of each antibody. Alternatively, at the time of tumour implantation, mice were intravenously administered adenoviral soluble VEGFR-3–Ig (ref. 46), or control adenovirus encoding β-galactosidase (1×10^9 p.f.u. per mouse). For analysis of the short-term effects on the vasculature and stroma of LNM35 or B16 tumours, tumour-bearing mice were treated for 6 days with AdVEGFR-3–Ig, antibodies and/or DAPT ($100 \, mg \, kg^{-1} \, d^{-1}$). Long-term effects were evaluated in LNM35 tumour-bearing mice by administering antibodies and/or DAPT ($75 \, mg \, kg^{-1} \, d^{-1}$) until the tumours reached a maximal size of 20 mm in diameter. Tumours were measured in x, y and z dimensions using a digital caliper, and volumes were calculated using the ellipse formula ($V = xyz/2$). Mice were given $60 \, mg \, kg^{-1}$ pimonidazole (Chemicon) intraperitoneally 1 h before they were killed.

Treatment of Rip1Tag2 transgenic mice with monoclonal antibodies. Altogether 12 Rip1Tag2 transgenic mice[35,36] were treated with $30 \, mg \, kg^{-1}$ anti-VEGFR-3, whereas 6 mice received anti-VEGFR-2 and 15 mice the control IgG every other day for two weeks. Mice were killed on day 14. For the analysis of blood vessel density and blood vessel functionality, mice were tail-vein-injected with $100 \, \mu l$ of $1 \, mg \, ml^{-1}$ fluorescein-labelled *Lycopersicon esculentum* lectin (Vector Laboratories) under inhalation-anaesthesia with isoflurane (Minrad Inc.). After 5 min, mice were perfused with 10 ml of 4% paraformaldehyde followed by 10 ml PBS. Isolated pancreata were immersed in ascending concentrations of sucrose (12%, 15% and 18%, for 1 h each), embedded in OCT (Tissue-Tek) and snap-frozen in liquid nitrogen. For the evaluation of blood vessel density, 10-μm sections were analysed with a Nikon Diaphot 300 immunofluorescence microscope using Openlab 3.1.7. Software (Improvision) and the number of fluorescein-labelled vessels in the tumours was determined using Image J software (The National Institutes of Health).

Superovulation. 24-day-old mice received an intraperitoneal injection of 5 international units (IU) pregnant mare serum gonadotropin (National Hormone and Peptide Program, Harbor-UCLA Medical Centre) followed by an injection of 5 IU human chorionic gonadotropin (Pregnyl) 47 h later. Mice were killed and ovaries collected for analysis 72 or 84 h after stimulation of superovulation.

Immunohistochemistry. 50-μm sections of tumours or ovaries, 80-μm cross-sections of the duodenum, and 7-μm sections of skin were fixed with cold acetone, washed with PBS and blocked with TNB (PerkinElmer). The following primary antibodies were used for immunostaining of mouse tissues: polyclonal goat anti-mouse VEGFR-3 (AF743, R&D Systems), rat-anti mouse VEGFR-3 (clone AFL4, 16-5988, eBioscience), polyclonal goat anti-mouse VEGFR-2 (AF644, R&D Systems), rat anti-mouse VEGFR-2 (clone AVAS-12α1, 550549, BD Biosciences), rat anti-mouse VEGFR-1 (clone 5B12, ImClone), polyclonal goat anti-mouse DLL4 (AF1389, R&D Systems), hamster anti-PECAM-1 (clone 2H8, MAB1398Z, Chemicon), unconjugated or FITC-conjugated rat anti-PECAM-1 (clone MEC 13.3, 557355 and 553372, BD Biosciences), FITC-conjugated CD11b (clone M1/70, 550282, BD Biosciences), polyclonal rabbit anti-FITC (71-1900, Zymed/Invitrogen), polyclonal rabbit anti-VEGF-C (6 and pre-immune serum[29]), rat anti-mouse VE-cadherin (clone 11D4.1, 550548, BD Biosciences) rat anti-mouse pan-endothelial antigen (clone MECA-32, 550563, BD Biosciences), polyclonal rabbit anti-cow GFAP (Z0334, Dako), rat anti-mouse F4/80 (clone BM8, BM4007, Acris antibodies), polyclonal rabbit anti-NG2 (AB5320, Chemicon), Cy3-conjugated mouse anti-SMA (clone 1A4, C6189, Sigma), polyclonal rabbit anti-LYVE-1 (ref. 31) and FITC-conjugated mouse anti-pimonidazole (Hypoxyprobe, HP2-1000, Chemicon). Human tissues were stained with mouse anti-human VEGFR-3 (clone 9D9, ref. 47), polyclonal rabbit anti-podoplanin[48], or polyclonal rabbit anti-human von Willebrand factor (A082, Dako). Sections were washed with TNT-buffer ($0.15 \, M$ NaCl, $0.1 \, M$ Tris-HCl, pH 7.5, 0.05% Tween20) and the primary antibodies were detected with the appropriate Alexa 488, 594 or 647 secondary antibody conjugates (Molecular Probes/Invitrogen). Bromodeoxyuridine (BrdU) was detected with Alexa 594-conjugated mouse anti-BrdU antibodies (Molecular Probes/Invitrogen) after incubation in hydrochloric acid and neutralization using sodium tetraborate. For whole-mount analysis of the cutaneous blood vessels, dermal tissues of the ear[43] or ventral skin of pups[49] were exposed for staining, as published. For analysis of the microvasculature, retinas were stained with biotinylated *Griffonia simplicifolia* lectin (isolectin B4, Vector Laboratories), as before[10], followed by immunostaining. Alternatively, retinas,

X-gal-stained *Vegfc*[+/LacZ] embryos or tumour sections were incubated in 5% hydrogen peroxide in methanol, followed by VEGFR-3 or PECAM-1 antibodies, biotinylated secondary antibodies (Vector Laboratories) and signal detection with the Avidin–Biotin Complex kit (Vector Laboratories)[50] or tyramide signal amplification (Perkin Elmer). Diaminobenzidine (Sigma or Chemicon) was used as the chromogen in both protocols. X-gal- and PECAM-1-stained *Vegfc*[+/LacZ] embryos were embedded in paraffin and sectioned in horizontal or sagittal orientation. Nuclear counterstaining was carried out with nuclear red[31].

The specificity of the goat anti-mouse VEGFR-3 antibody (R&D Systems) to VEGFR-3 was verified by whole-mount staining of VEGFR-3-knockout embryos collected at E9, and compared with wild-type embryos (Supplementary Fig. 6c and data not shown). We observed specific staining in the vessels in wild-type embryos, whereas no staining could be observed in VEGFR-3-deficient embryos, indicating that the VEGFR-3 antibody used in the study was indeed specific for VEGFR-3.

All fluorescently labelled samples were mounted with Vectashield mounting medium containing 4,6-diamidino-2-phenylindole (DAPI; H-1200, Vector Laboratories), and analysed with a compound fluorescent microscope (Zeiss 2, Carl Zeiss; ×10 objective with numerical aperture 0.30) or a confocal microscope (Zeiss LSM 510, oil objectives ×40 with NA 1.3 and ×63 with NA 1.4) by using multichannel scanning in frame mode. The pinhole diameter was set at 1 Airy unit for detection of the Alexa 488 signal, and was adjusted for identical optical slice thickness for the fluorochromes emitting at higher wavelengths. Three-dimensional projections were digitally reconstructed from confocal *z*-stacks. Co-localization of signals was assessed from single confocal optical sections. Images of whole embryos were acquired using tile scanning using a pinhole diameter >3.0 Airy units. X-gal staining of LacZ reporter mice was carried out as published[31], and samples were mounted in Aquamount (BDH Laboratory Supplies) or Vectashield mounting medium containing DAPI. Co-localization of the β-galactosidase chromogen and the fluorescent signal was carried out as described previously[13].

Analysis of kidney pathology and function. NMRI mice received anti-VEGFR-3, anti-VEGFR-2 or non-specific rat IgG (40 mg kg^{-1} every other day), or both anti-VEGFR-3 and anti-VEGFR-2 (40 mg kg^{-1} of each antibody every other day), for 10 days ($n \geq 3$). Mice were killed and urine was collected by bladder puncture using a 33-gauge needle. Proteinuria was assessed by pipetting 10 μl of urine on colour-coded strips (Combur 3 Test Strips, Roche). We did not observe significant proteinuria in the mice by this method (data not shown). Albuminuria was measured using an indirect ELISA kit for detection of mouse albumin (Albuwell M, Exocell) according to the manufacturer's instructions. The albumin levels were normalized to urine creatinine levels using a direct ELISA assay (R&D Systems). Kidneys were collected, cut in half in the horizontal plane at the pyloric midline, fixed and embedded in paraffin. Paraffin sections were stained with haematoxylin/eosin or PECAM-1 antibodies, and observed under a bright field microscope. For transmission electron microscopy (TEM), at least three antibody-treated NMRI mice or K14–VEGFR-3–Ig transgenic mice were perfusion-fixed with 4% formaldehyde in 100 mM phosphate buffer, pH 7.4, and slices of kidney were incubated in the same fixative overnight (16 h) at +10 °C. Samples were then fixed with 2% glutaraldehyde in the same buffer for 1 h, and post-fixed with 1% buffered osmium tetroxide for 1 h, dehydrated and embedded in epon at room temperature (+22 °C). Sections were post-stained with uranyl acetate and lead and were examined with a Jeol EX1200 II TEM operating at 60 kV. Images were acquired with an ES500W CCD camera (Gatan Corp.).

Vessel morphometry and quantitative analysis. The vascular surface area in retinas was quantified as an isolectin B4-positive area from ×10 confocal micrographs of all intact quarters of the processed retina using Image J software, as described previously[42,43]. PECAM-1-positive vessels in the ears or the LYVE-1-positive vessel area in the intestines were quantified in a similar manner. VEGFR-3-positive surface area was normalized to isolectin B4 surface area from double-stained retinas to yield the percentage of VEGFR-3-positive vessels. Vessel branching points and sprouts were counted manually as in ref. 14, and their number was normalized to the area of retina analysed. This analysis was carried out from 22 anti-VEGFR-3-, 18 anti-VEGFR-2-, 24 IgG- and 12 anti-VEGFR-3 plus anti-VEGFR-2-treated retinas from four separate experiments. BrdU-positive endothelial cells were counted manually from ×10 confocal *z*-stacks of BrdU and isolectin B4 double-stained retinas. Again, all intact quarters of the retina were used for analysis. Endothelial sprout number and length was counted from fluorescent micrographs of *Dll4*^{+/−} heterozygous retinas, as described previously[16]. Four *Dll4*^{+/−} mice received anti-VEGFR-3, three received anti-VEGFR-2 and two received control IgG.

The embryos were staged at E8.5–E9.5 according to the Edinburgh Mouse Atlas criteria. Six litters at E8.5 ($n = 6$ −/−, 6 +/+), six litters at E9.0 ($n = 8$ −/−, 10 +/+) and three litters at E9.5 ($n = 5$ −/−, 5 +/+) were analysed. The

number of vessel branching points was manually counted from ×10 confocal stacks in the head at E8.5, where one layer of vessels can be seen (Supplementary Fig. 6a). Again, the criteria used in ref. 14 were applied. The length and area of intersomitic vessels from between somites 12 and 15 was quantified from ×10 micrographs obtained with the pinhole open.

Tumour vasculature was analysed from thick sections stained with PECAM-1 antibodies. At least three 0.81 mm^2 or 1.69 mm^2 micrographs from regions of uniform staining intensity were acquired, and vascular surface area was quantified using Image J software. According to our analysis, all vessel sprouts in LNM35 tumours were VEGFR-3-positive, whereas most sprouts expressed low levels of the junctional protein PECAM-1. As a result, we used VEGFR-3 as a marker for sprouts in tumours. The sprouts were counted manually from LNM35 tumour sections from regions in parts of the tumour that did not contain LYVE-1-positive lymphatic vessels[22]. VEGFR-3 did not co-localize with pericyte markers (smooth muscle actin, PDGFR-β, NG2), nor was it expressed by any of the tumour cells analysed[22], or by Rip1Tag2 insulinoma cells (data not shown). Approximately 5% of cells expressing the macrophage/monocyte marker CD11b were also VEGFR-3-positive. Vessels positive for lectin were counted from Rip1Tag2 tumour sections. Images were edited using PhotoShop software (Adobe).

Real-time quantitative PCR. RNA was isolated from retinas using the RNeasy Micro Kit (Qiagen, 74004). Homogenization was performed using rotor-stator homogenization, followed by disruption using a shredder column (Qiagen, 79656) and on-column DNase digestion. Samples were quality controlled on an Agilent 2100 Bioanalyser using the Agilent 2100 Expert software (version B.02.02.SI238) and the Agilent RNA 6000 Nano Kit (5067-1511). Two separate *in vitro* transcription reactions were performed from every RNA sample using the SuperScript III First-Strand Synthesis Kit for real-time (RT)–PCR (Invitrogen, 18080-051) according to the manufacturer's instructions. Three RT quantitative PCR reactions/TaqMan assays were carried out from every *in vitro* transcription reaction using TaqMan Universal PCR Master Mix (43004437, Applied Biosystems) and the 7300 Real Time PCR System (Applied Biosystems) according to a standardized protocol[13]. The TaqMan Assays (Applied Biosystems) used: *Gapdh* (4352932E), *Cadh5* (Mm00486938_m1), *Pdgfb* (Mm00440678_m1), *Vegfr2* (Mm001222419_m1), *Vegfr3* (Mm00433337_m1), *Nrarp* (Mm00482529_s1), *Vegfa* (Mm00437304_m1), *Hey1* (Mm00468865_m1), *Hey2* (Mm00469280_m1) and *Hes1* (Mm00456108_g1). Using the Sequence Detection System (version 1.4, Applied Biosystems), the data were normalized to the endogenous control *Gapdh*, and fold changes were calculated using the comparative CT method. In the case of *Vegfr3* and *Pdgfb* in DAPT-treated retinas, relative fold changes in *Cadh5* were used to control for increased endothelial cell numbers in the sample (Supplementary Fig. 10h). At least three retinas from pups treated with DAPT, JAG1, SC-JAG1 or DAPT vehicle (10% ethanol, 90% sunflower oil) from each time point (6 h, 12 h, 24 h and 48 h) were used for analysis at P5. The contralateral retina was analysed by VEGFR-3 immunofluorescence and isolectin B4 staining. Altogether three retinas from DLL4 heterozygous (*Dll4*^{+/−}) and five retinas from wild-type littermate pups (*Dll4*^{+/+}) were used for the analysis.

Statistical analysis. At least six animals were used for each analytical time point and technique studied. Representative data from at least three replicate experiments are shown, with the exception of the experiments involving *Dll4*^{+/−} mice and the Rip1Tag2 transgenic mice. A two-tailed Student's *t*-test or two-way ANOVA was used for statistical analysis. A *P* value of less than 0.05 was considered to be statistically significant, and is indicated with an asterisk in the figures.

31. Karkkainen, M. J. *et al.* Vascular endothelial growth factor C is required for sprouting of the first lymphatic vessels from embryonic veins. *Nature Immunol.* **5**, 74–80 (2004).
32. Duarte, A. *et al.* Dosage-sensitive requirement for mouse Dll4 in artery development. *Genes Dev.* **18**, 2474–2478 (2004).
33. Kiba, A., Sagara, H., Hara, T. & Shibuya, M. VEGFR-2-specific ligand VEGF-E induces non-edematous hyper-vascularization in mice. *Biochem. Biophys. Res. Commun.* **301**, 371–377 (2003).
34. Zheng, Y. *et al.* Chimeric VEGF-ENZ7/PlGF promotes angiogenesis via VEGFR-2 without significant enhancement of vascular permeability and inflammation. *Arterioscler. Thromb. Vasc. Biol.* **26**, 2019–2026 (2006).
35. Hanahan, D. Heritable formation of pancreatic beta-cell tumours in transgenic mice expressing recombinant insulin/simian virus 40 oncogenes. *Nature* **315**, 115–122 (1985).
36. Esni, F. *et al.* Neural cell adhesion molecule (N-CAM) is required for cell type segregation and normal ultrastructure in pancreatic islets. *J. Cell Biol.* **144**, 325–337 (1999).
37. Pytowski, B. *et al.* Complete and specific inhibition of adult lymphatic regeneration by a novel VEGFR-3 neutralizing antibody. *J. Natl Cancer Inst.* **97**, 14–21 (2005).

38. Prewett, M. *et al.* Antivascular endothelial growth factor receptor (fetal liver kinase 1) monoclonal antibody inhibits tumor angiogenesis and growth of several mouse and human tumors. *Cancer Res.* **59**, 5209–5218 (1999).

39. Dovey, H. F. *et al.* Functional gamma-secretase inhibitors reduce β-amyloid peptide levels in brain. *J. Neurochem.* **76**, 173–181 (2001).

40. Weijzen, S. *et al.* The Notch ligand Jagged-1 is able to induce maturation of monocyte-derived human dendritic cells. *J. Immunol.* **169**, 4273–4278 (2002).

41. Enholm, B. *et al.* Adenoviral expression of vascular endothelial growth factor-C induces lymphangiogenesis in the skin. *Circ. Res.* **88**, 623–629 (2001).

42. Wirzenius, M. *et al.* Distinct vascular endothelial growth factor signals for lymphatic vessel enlargement and sprouting. *J. Exp. Med.* **204**, 1431–1440 (2007).

43. Tammela, T. *et al.* Angiopoietin-1 promotes lymphatic sprouting and hyperplasia. *Blood* **105**, 4642–4648 (2005).

44. Kozaki, K. *et al.* Establishment and characterization of a human lung cancer cell line NCI-H460–LNM35 with consistent lymphogenous metastasis via both subcutaneous and orthotopic propagation. *Cancer Res.* **60**, 2535–2540 (2000).

45. Sakai, K. *et al.* Expression and function of class II antigens on gastric carcinoma cells and gastric epithelia: differential expression of DR, DQ, and DP antigens. *J. Natl Cancer Inst.* **79**, 923–932 (1987).

46. Karpanen, T. *et al.* Vascular endothelial growth factor C promotes tumor lymphangiogenesis and intralymphatic tumor growth. *Cancer Res.* **61**, 1786–1790 (2001).

47. Jussila, L. *et al.* Lymphatic endothelium and Kaposi's sarcoma spindle cells detected by antibodies against the vascular endothelial growth factor receptor-3. *Cancer Res.* **58**, 1599–1604 (1998).

48. Kriehuber, E. *et al.* Isolation and characterization of dermal lymphatic and blood endothelial cells reveal stable and functionally specialized cell lineages. *J. Exp. Med.* **194**, 797–808 (2001).

49. Karpanen, T. *et al.* Lymphangiogenic growth factor responsiveness is modulated by postnatal lymphatic vessel maturation. *Am. J. Pathol.* **169**, 708–718 (2006).

50. Saaristo, A. *et al.* Lymphangiogenic gene therapy with minimal blood vascular side effects. *J. Exp. Med.* **196**, 719–730 (2002).